Appendix: Supplementary Information

Coral geochemical signals and growth responses to coseismic uplift during the great Sumatran megathrust earthquakes of 2004 and 2005

Saori Ito, Atsuko Yamazaki, Yuichi Nishimura, Eko Yulianto, Tsuyoshi Watanabe

Summary of this supplementary file:

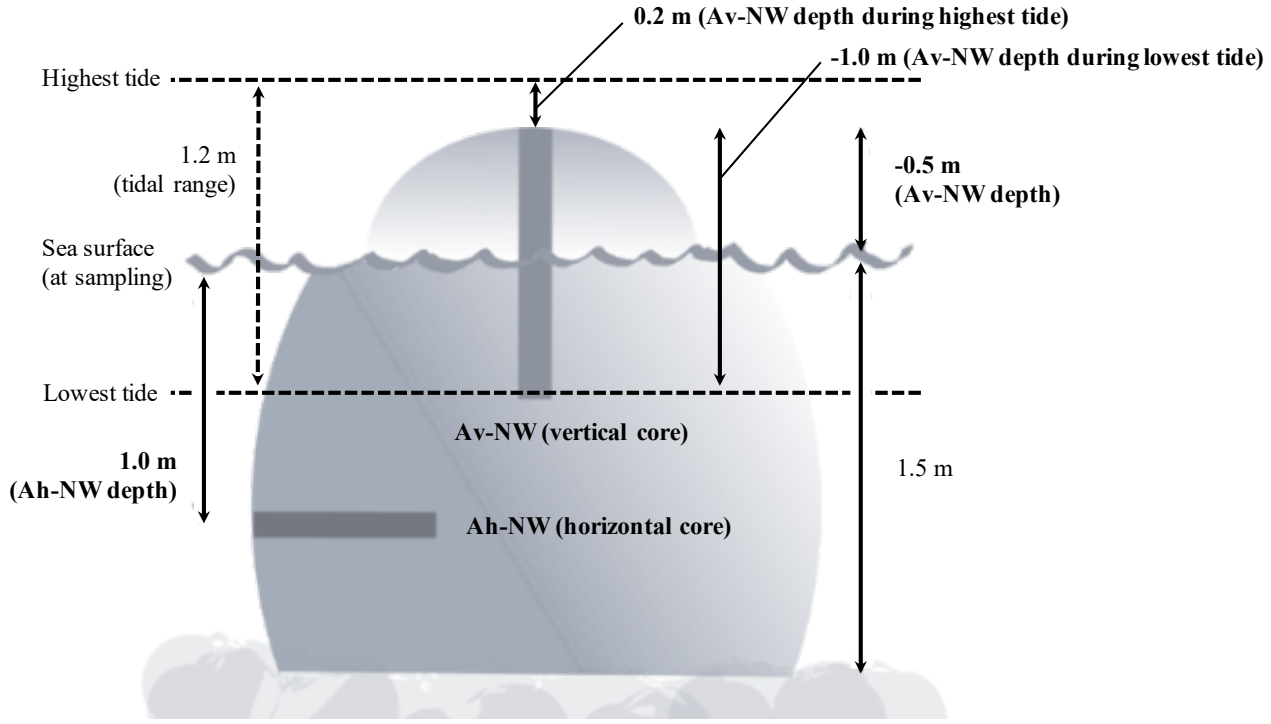

Fig. S1 Sample positions of Av-NW and Ah-NW

Av-NW (vertical core) and Ah-NW (horizontal core) are from a single colony. The values (in m) with bold character mean water depth of each core top at core drilling. The dashed lines show the highest or lowest tide (1.2 m tidal range). “Depth during highest/lowest tide” was estimated in the basis on water depth and the tidal range (see also Table 1).

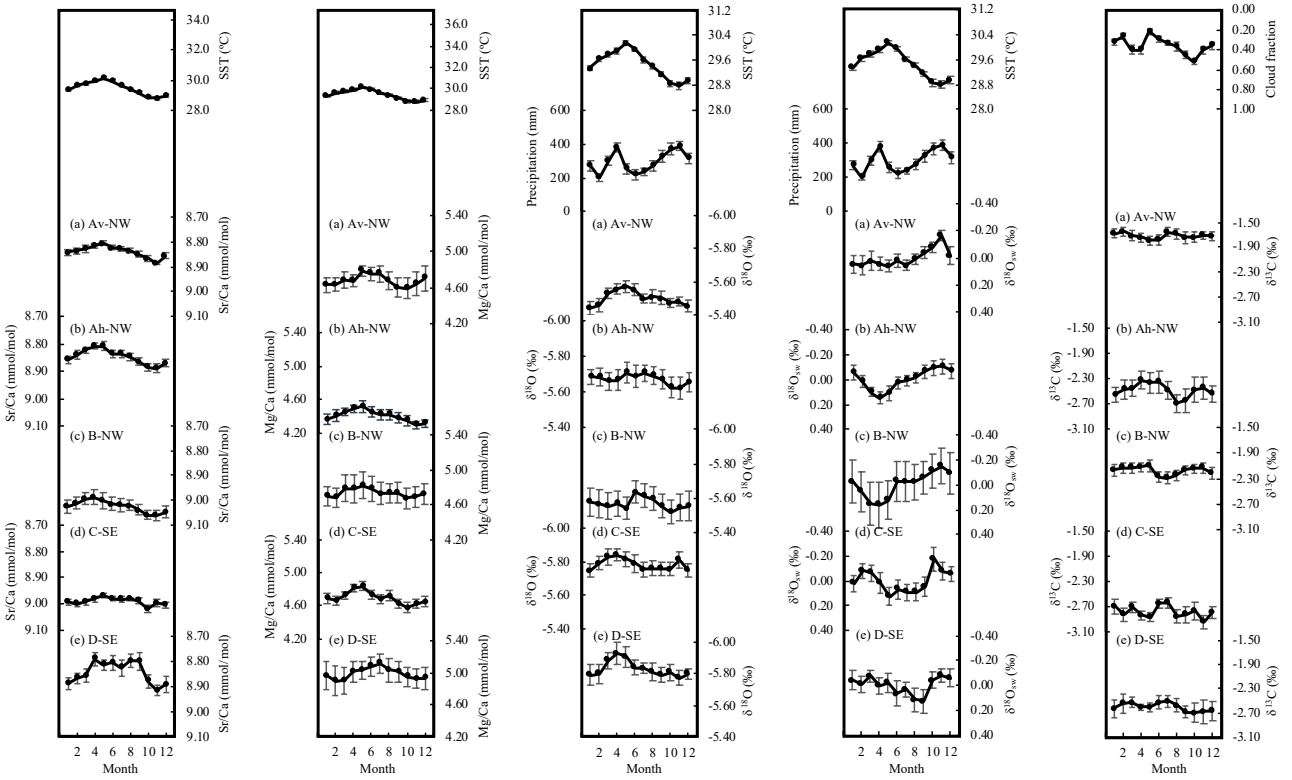

Fig. S2 Seasonal trends of environmental data (SST, precipitation, and cloud fraction) and geochemical data

The monthly IGOSS-SST was derived from the Integrated Global Ocean Services System Products Bulletin. The monthly precipitation data was derived from WCRP GCOS GPCC Monitoring. Cloud fraction data (1 = covered with cloud completely) was derived from FRESCO+ SCIAMACHY. All the geochemical records were resampled monthly resolution. Each y-axis range in SST was determined by the variable range in the geochemical proxy as follows: Sr/Ca was 0.4 mmol/mol which is equivalent to 6.6 ºC (Abram et al., 2007), Mg/Ca was 1.2 mmol/mol which is equivalent to 9.3 ºC (Mitsuguchi et al., 1996), and $\delta^{18}O$ was 0.6 ‰, which is equivalent to 3.2 ºC (Abram et al., 2007). The error bars show standard errors. Estimated $\delta^{18}O_{sw}$ was calculated from skeletal Sr/Ca and $\delta^{18}O$ (Juillet-Leclerc and Schmidt, 2001; Cahyarini et al., 2008).

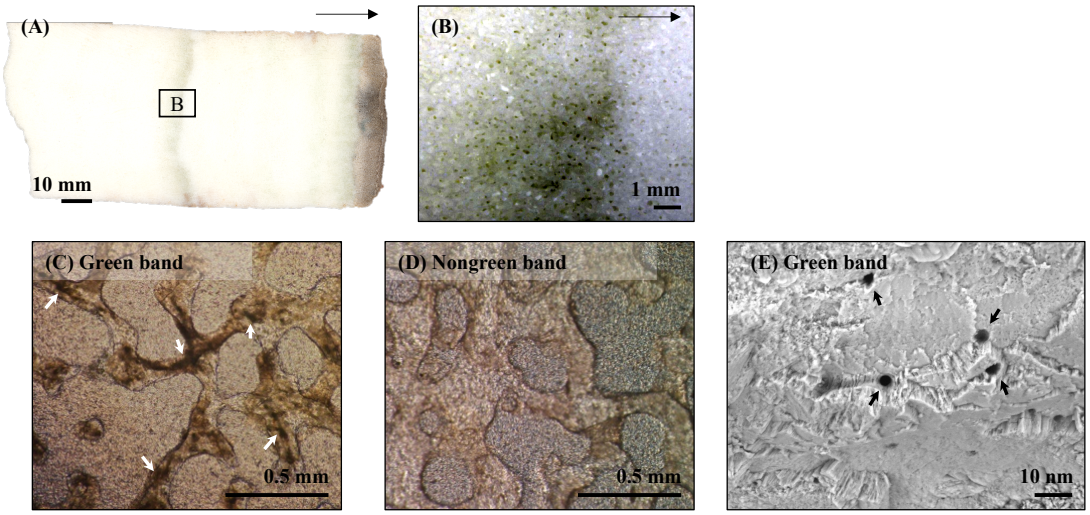

Fig. S3 Green band created by endolithic algae on the D-SE slab surface

(A) 8 mm green band on the D-SE slab surface. The arrow shows the growth direction. (B) The microscopic picture of the green band area "B" on figure (A). (C) (D) A part of the green band and nongreen band shown under a microscope (thin sections). The skeletal structure of nongreen band area was clear (D), while the skeletal structure of the green band area would contain the endolithic algae (C; white arrows; e.g., *Ostreobium* spp.). (E) Trace of microbioerosion due to microboring by endolithic algae (black arrows), shown under an electron microscope (cross section of the green band). *Ostreobium* spp. left the 3-5 nm microboring which conform to the shape of their thallic (filament).

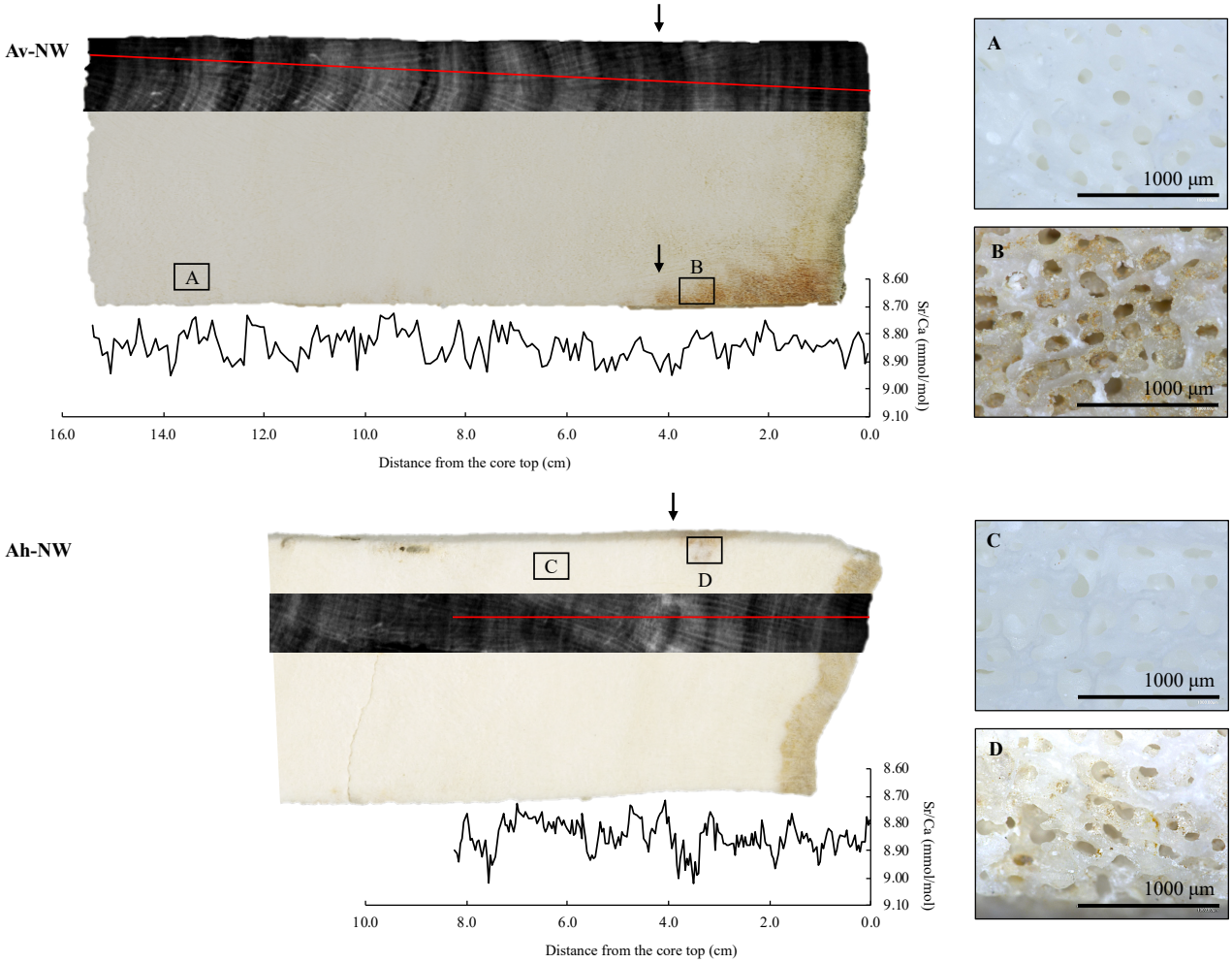

Fig. S4 Incorporation of suspended small particles on the Av-NW and Ah-NW skeleton

The X-ray images (negative) are combined with the slab images. The slab images were taken after microsampling (Ah-NW slab has cracked during microsampling). The black arrows show the occurrence of the 2004 earthquake (and tsunami). (A) and (C) are parts of the pre-earthquake shown under a microscope, which indicates a normal slab surface. (B) and (D) are parts of the post-earthquake shown under a microscope, which indicates incorporation of small particles like clay minerals in the skeleton. X-radiographs did not show the anomalous high or low density on the (B) and (C) area (compared by Fig. 2).

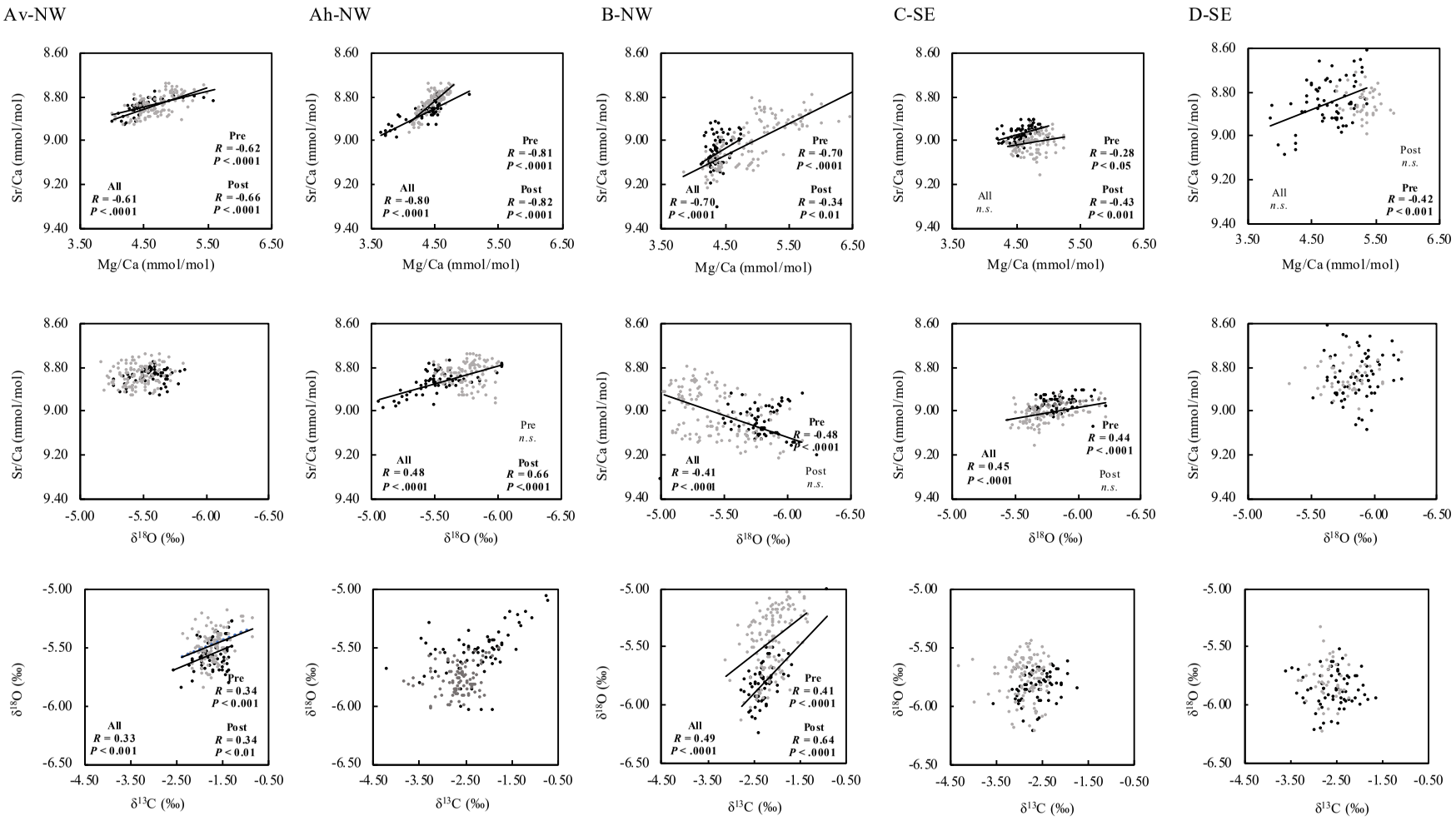
Av-NW
Ah-NW
B-NW
C-SE
D-SE
Sr/Ca (mmol/mol)
Mg/Ca (mmol/mol)
δ18O (‰)
δ13C (‰)
All
Pre
Post
n.s.

Fig. S5 Plots of skeletal geochemical proxies (Sr/Ca vs. Mg/Ca, Sr/Ca vs. $\delta^{18}O$, and $\delta^{18}O$ vs. $\delta^{13}C$)

Plots were resampled monthly resolution (the last 4 data points of the Mg/Ca record in Av-NW were excluded because these 4 data showed anomalous change due to air-exposed stress). The gray plots show the data in pre-earthquakes (from the oldest date to November 2004, and the black plots show the data in post-earthquakes (from December 2004 to the date of core drilling). When the significant relationship is available, *R* value (a correlate coefficient value) and *P* value (a statically significant *P* value for the Student's t-test) are shown on the graph with "Pre," "Post," or "All (through both pre- and post-earthquakes periods)."

(a) Av-NW

	Sr/Ca	Mg/Ca	$\delta^{18}O$	$\delta^{13}C$
SST	-0.95***	0.67*	-0.75**	-0.28
Precipitation	0.55**	-0.49	0.05	-0.25
Cloud fraction	0.59*	-0.68*	0.23	-0.02

(b) Ah-NW

	Sr/Ca	Mg/Ca	$\delta^{18}O$	$\delta^{13}C$
SST	-0.96***	0.95***	-0.73**	0.53
Precipitation	0.42	-0.38	0.80**	0.03
Cloud fraction	0.55	-0.47*	0.74**	-0.30

(c) B-NW

	Sr/Ca	Mg/Ca	$\delta^{18}O$	$\delta^{13}C$
SST	-0.93***	0.79**	-0.42	0.02
Precipitation	0.41	-0.17	0.60*	0.40
Cloud fraction	0.49	-0.39	0.42	0.08

(d) C-SE

	Sr/Ca	Mg/Ca	$\delta^{18}O$	$\delta^{13}C$
SST	-0.75**	0.87**	-0.54	0.27
Precipitation	0.36	-0.25	-0.21	-0.49
Cloud fraction	0.58*	-0.59*	0.15	-0.10

(e) D-SE

	Sr/Ca	Mg/Ca	$\delta^{18}O$	$\delta^{13}C$
SST	-0.64*	0.42	-0.80**	0.74**
Precipitation	0.25	-0.31	<-0.01	-0.73**
Cloud fraction	0.15	-0.22	0.24	-0.56*

* $P < 0.05$; ** $P < 0.01$; *** $P < .0001$

94

95 **Table S1 Correlation coefficient *R* value between environmental data and geochemical records**

96 All environmental data and geochemical data were a monthly resolution (see also Fig. S2). The "*P*"

97 is a statically significant *P* value for the Student's t-test.

Evidence	Av-NW	Ah-NW	B-NW	C-SE	D-SE
(a) Seasonal cycle range (mmol/mol)					
Skeletal Sr/Ca	0.09	0.08	0.07	0.05	0.13
Skeletal Mg/Ca	0.28	0.22	0.15	0.27	0.22
Skeletal $\delta^{18}O$	0.13	0.09	0.12	0.09	0.16
(b) Skeletal Sr/Ca vs IGOSS-SST (*R*-value; * $P < 0.05$; ** $P < 0.01$; *** $P < .0001$)					
	-0.95^{***}	-0.96^{***}	-0.93^{***}	-0.75^{**}	-0.64^{*}
(c) The 1997 Indian Ocean Dipole Signal in the skeletal Sr/Ca record					
	○	○	○	○	No data
(d) The 2004 earthquake and tsunami occurrence signals on the coral skeleton					
Stress band	-	○	-	○	-
Green band	-	-	-	-	○
Small particles like clay materials	○	○	-	-	-
(e) Annual extension rate (mm/yr)					
	10.69	6.12	10.19	25.26	11.98

Table S2 Cross-checking and the evidence of age models

(a) The seasonal trend of each geochemical record is shown in Fig S2. In our study site, an annual amplitude of SST observed on IGOSS-SST (1.5 °C on average) should be equal to 0.09 mmol/mol (Abram et al., 2007), 0.19 mmol/mol (Mitsuguchi et al., 1996), and 0.28 ‰ (Abram et al., 2007) range in an annual cycle for skeletal Sr/Ca, Mg/Ca, $\delta^{18}O$ based on each proxy-SST dependency, respectively. In skeletal Sr/Ca, the seasonal cycle in Av-NW, Ah-NW, and B-NW showed a clear annual cycle with valid range, while the C-SE and D-SE record fluctuated more than are expected from SST cause. The annual cycle in skeletal Sr/Ca of D-SE was not clear, while the annual bands were clearly visible on the X-ray image (Fig. 2). In skeletal Mg/Ca, the annual cycle range in our records did not agree with the skeletal Mg/Ca-SST dependency estimated by the previous study. Our skeletal Mg/Ca record fluctuated more than are expected from SST cause because of the complexity of the controlling factors (e.g., Watanabe et al. 2001; Nagtegaal et al. 2012). In skeletal $\delta^{18}O$, the annual cycle range in our records did not agree with the skeletal $\delta^{18}O$-SST dependency estimated by the previous

study. These small seasonal amplitudes of skeletal $\delta^{18}O$ would be caused by salinity changes (Cole and Fairbanks, 1990; Carriquiry et al., 1994; Al-Rousan et al., 2007; McCulloch et al., 1999). Skeletal $\delta^{18}O$ reflects both SST and seawater oxygen isotopes ($\delta^{18}O_{seawater}$: positively correlated with salinity). In our sample sites, salinity variations (32.4–34.3 psu for CARTON-GIESE SODA data, from June 1994 to December 2008 at 2.25 N, 95.25 E with 5.01 m depth; and 33.0-34.9 for Aquarius IPRC/SOEST OISSS data, from September 2011 to May 2015 at 2.3 N, 95.3 E) are equal to 0.80 ‰ in $\delta^{18}O_{seawater}$, based on the salinity-$\delta^{18}O_{seawater}$ slope (0.42 $‰_{VSMOW}$ / psu: Morimoto et al., 2002). Thus, the small seasonal amplitude of SST components for skeletal $\delta^{18}O$ (0.28 ‰, equal to 1.5 °C) could be masked by $\delta^{18}O_{seawater}$ variations due to evaporation or freshwater input (i.e., precipitations, input from the river). (b) *R*- and *P*-values are shown in Table S1. Skeletal Sr/Ca significantly correlated with monthly SST in all coral cores. It suggests that skeletal Sr/Ca record reflects SST variation. (c) The skeletal Sr/Ca records are shown in Figure 3. The extreme Indian Ocean Dipole (IOD) signal in 1997 was found in the skeletal Sr/Ca records in all cores (the D-SE was excluded because of no data). The 1997 IOD signal in the skeletal Sr/Ca provides the precision of the age model. (d) The 2004 earthquake and tsunami signals: a stress band (inshore corals; Fig. 2), a green band (D-SE; Fig. S3), and an incorporation of the small particles like clay materials (Av-NW and Ah-NW; Fig. S4) were observed on the coral skeleton. These signals are evidence of the precise age model. (e) The annual skeletal extension rate (mm/yr) was assumed to be constant between dates of the adjacent highest Sr/Ca (i.e., age model). The 6.12-25.26 mm/yr of annual extension rate for *Porites* coral agrees with previous studies (e.g., Lough and Barnes, 2000; Scoffin et al., 1992; Goodkin et al., 2012; Watanabe et al., 2017).

Post-earthquake period	$\Delta\delta^{13}C$ (‰)	ΔSr/Ca (mmol/mol)	ΔMg/Ca (mmol/mol)	$\Delta\delta^{18}O$ (‰)
(a) Av-NW				
from the 2004 earthquake	-0.08	0.05	-0.14*	-0.10**
from the 2005 earthquake	-0.11	<-0.01	-0.08	-0.08*
(b) Ah-NW				
from the 2004 earthquake	0.34**	0.04***	-0.05	0.21***
from the 2005 earthquake	0.30*	0.04***	-0.01	0.19***
(c) B-NW				
from the 2004 earthquake	-0.17*	0.05***	-0.53***	-0.34***
from the 2005 earthquake	-0.16*	0.06***	-0.53***	-0.33***
(d) C-SE				
from the 2004 earthquake	0.34***	-0.04***	-0.16***	-0.08***
from the 2005 earthquake	0.32***	-0.04***	-0.15***	-0.09***
(e) D-SE				
from the 2004 earthquake	0.14	-0.02	-0.46***	-0.03
from the 2005 earthquake	0.08	-0.01	-0.47***	-0.01

* $P < 0.05$; ** $P < 0.01$; *** $P < .0001$

Table S3 Comparison of Δ*Proxy* in two post-earthquake periods

The post-earthquake period means from the 2004 or 2005 earthquake to the date of core drilling. The "*P*" is a statically significant *P* value for the Student's t-test.

(a) Av-NW

	Sr/Ca	Mg/Ca	$\delta^{18}O$	$\delta^{13}C$
Extension rate	-0.15	-0.25	0.07	-0.20
Density	0.08	-0.28	0.26	-0.20

(b) Ah-NW

	Sr/Ca	Mg/Ca	$\delta^{18}O$	$\delta^{13}C$
Extension rate	0.08	0.20	0.37	0.17
Density	0.06	-0.28	0.34	-0.13

(c) B-NW

	Sr/Ca	Mg/Ca	$\delta^{18}O$	$\delta^{13}C$
Extension rate	0.07	0.19	0.25	0.18
Density	-0.69^{**}	0.69^{**}	0.45	-0.02

(d) C-SE

	Sr/Ca	Mg/Ca	$\delta^{18}O$	$\delta^{13}C$
Extension rate	-0.46	-0.39	-0.15	0.80^{**}
Density	0.28	-0.23	0.19	-0.25

(e) D-SE

	Sr/Ca	Mg/Ca	$\delta^{18}O$	$\delta^{13}C$
Extension rate	-0.57	-0.04	-0.21	0.42
Density	0.02	-0.38	0.29	-0.36

$^{*}P < 0.05$; $^{**}P < 0.01$

Table S4 Correlation coefficient *R* value between annual skeletal growth parameters (skeletal extension rate and skeletal density) and annual mean of geochemical records

The analyzed period was1996 to 2009, 1997 to 2009, 1995 to 2009, 1997 to 2009, and 2002 to 2009 for Av-NW, Ah-NW, B-NW, C-SE, and D-SE, respectively. The "*P*" is a statically significant *P* value for the Student's t-test. There was no significant correlation between annual skeletal growth parameters and annual mean of geochemical records, excluding in B-NW (Sr/Ca vs. density and Mg/Ca vs. density) and in C-SE ($\delta^{13}C$ vs. extension rate). These significant correlations seem to be affected by the large deviation in skeletal extension rate and density (shown in Table S4, "SD").

Sample	Extension rate (mm/yr)		Density (g/cm^3)		Calcification rate ($g*cm^{-2}/yr$)	
	Mean	SD	Mean	SD	Mean	SD
Av-NW	10.69	3.99	1.27	0.11	1.52	0.53
Ah-NW	6.12	1.54	1.40	0.13	0.85	0.20
B-NW	10.19	2.56	1.30	0.17	1.25	0.37
C-SE	25.26	5.79	0.89	0.04	2.10	0.50
D-SE	11.98	2.34	1.41	0.09	1.54	0.32

143

144 **Table S5 Mean and standard deviation value for skeletal growth parameters**

145 Calculation methods for extension rate, density, and calcification rate were shown in the main text.

146 "SD" means standard deviation value.

Supplementary Text: S1. Age models

1. Methodology developing time series

As explained in the text, the age determination of each coral was based on the relationship between skeletal Sr/Ca and monthly SST (IGOSS-SST: 1° × 1° grid data at 2.5 N, 95.5 E). This monthly IGOSS-SST dataset from June 1994 to May 2010 showed a seasonal SST cycle with a small amplitude of 1.5 °C on average (SD: 0.4 °C). We used tie points to connect the highest (lowest) Sr/Ca values to the coolest (warmest) SST record to establish each year. The growth rate was assumed to be constant during each of the tied points. In a part of Sr/ca records of B-NW, C-SE, and D-SE, it was difficult to confirm that the maximum (minimum) peak corresponding to the minimum (maximum) SST. In this case, the chronologies were inserted by combining the skeletal Sr/Ca with annual density band patterns (Fig. 2).

2. Cross-check and the multiple "proof points" for the accuracy of age models

The age models of all coral cores were cross-checked through the characteristics of the geochemical records, the relationships between skeletal Sr/Ca and IGOSS-SST data, the 2004 earthquake and tsunami signals on the coral skeleton, and the skeletal growth parameters (see Table S2). There are multiple "proof points" for the accuracy of age model, for example, clear annual cycle with valid range in skeletal Sr/Ca (Av-NW, Ah-NW, and B-NW, Fig. S2), the strong positive correlation between skeletal Sr/Ca and monthly IGOSS-SST (all coral cores, Table S2), the IOD signal in skeletal Sr/Ca record (all coral cores, D-SE is no data, Fig. 3), the 2004 earthquake and tsunami occurrence signals on the coral skeleton (a stress band for Ah-NW and C-SE, Fig.2; a green band for D-SE, Fig. S3; and small particles like clay materials for Av-NW and Ah-NW, Fig. S4), the annual extension rate consistent with previous studies (all coral cores, Figs. S6 and S7), and the clear density bands (D-SE, Fig. 2). This evidence certifies that the age models are correct.

(1) Skeletal Sr/Ca

Skeletal Sr/Ca significantly correlated with monthly SST in all coral cores (Table S1). In our study

site, an annual amplitude of SST observed on IGOSS-SST (1.5 °C on average) should be equal to 0.09 mmol/mol range in an annual cycle, based on skeletal Sr/Ca-SST dependency (Abram et al., 2007). As shown in Fig. S2 and Table S2, skeletal Sr/Ca in Av-NW and Ah-NW indicated a clear annual cycle with the range of 0.09 and 0.08 mmol/mol. Skeletal Sr/Ca in B-NW and C-SE also showed an annual cycle with the range of 0.07 and 0.05 mmol/mol. The annual cycle in skeletal Sr/Ca of D-SE was not clear (with the range of 0.13 mmol/mol), while the annual bands were clearly visible on the X-ray image (Fig. 2). Thus, the results of Table S1, Figure S2, the IOD signal in skeletal Sr/Ca record, clear density bands (D-SE), and the skeletal signal of earthquake occurrence provides strong evidence that the age models are correct. Moreover, the extreme Indian Ocean Dipole (IOD) signal in 1997 was found in the skeletal Sr/Ca records, excluding D-SE (no data), and the signal was used as a guide to making the age models. The IOD is an interannual, aperiodic oscillation of sea-surface temperatures in the equatorial Indian Ocean. Therefore, the IOD signal in skeletal Sr/Ca record was one of the evidence of the precision of the age model.

(2) Skeletal “pin-point” signals of the 2004 earthquake and tsunami occurrence

A stress band (inshore corals, Ah-NW and C-SE, Fig. 2), a green band (D-SE, Fig. S3), and an incorporation of the small particles like clay materials (Av-NW and Ah-NW, Fig. S4) were confirmed as the skeletal “pin-point” signals of the 2004 earthquake and tsunami occurrence. These signals are the guides for the precise age models.

(3) Skeletal extension rate

Our results of skeletal growth parameters were also cross-checked by comparison with previous studies (Lough & Barnes, 2000; Scoffin et al., 1992; Goodkin et al., 2012). Figs. S6 and S7 indicate that all of our records agree with the previous studies. Especially in Fig. S6-a *Density vs. Extension rate*, it suggests that the chronologies and extension rates for our coral cores must be correct because these growth parameters are independent variables. The annual skeletal extension rate (mm/yr) was assumed to be constant between dates

of the adjacent highest Sr/Ca (i.e., age model). The skeletal density (g/cm^3) was calculated based on the X-ray photographs of coral cores. Therefore, Fig. S6-a provides good evidence that the chronologies and skeletal extension rates for our coral cores are correct. Besides, the C-SE has a relatively fast extension rate (Fig. 4 and Table S4, the mean value: 25.3 mm/yr, the range: 18.4–34.4 mm/yr). The skeletal extension rate in C-SE was cross-checked by comparison with annual SST, based on Goodkin et al. (2012). Our *Porites* coral core C-SE agrees with the relationship between the skeletal extension rate and annual SST (Fig. S7). It suggests that the extension rate for C-SE must be correct. Moreover, Watanabe et al. (2017) reported that the Oman coral grew very quickly, on average 25.1 mm/year with a range between 19 to 31.5 mm/year. Thus, our skeletal extension rates agreed with the previous studies, and these results provide strong evidence of the precision of the age model.

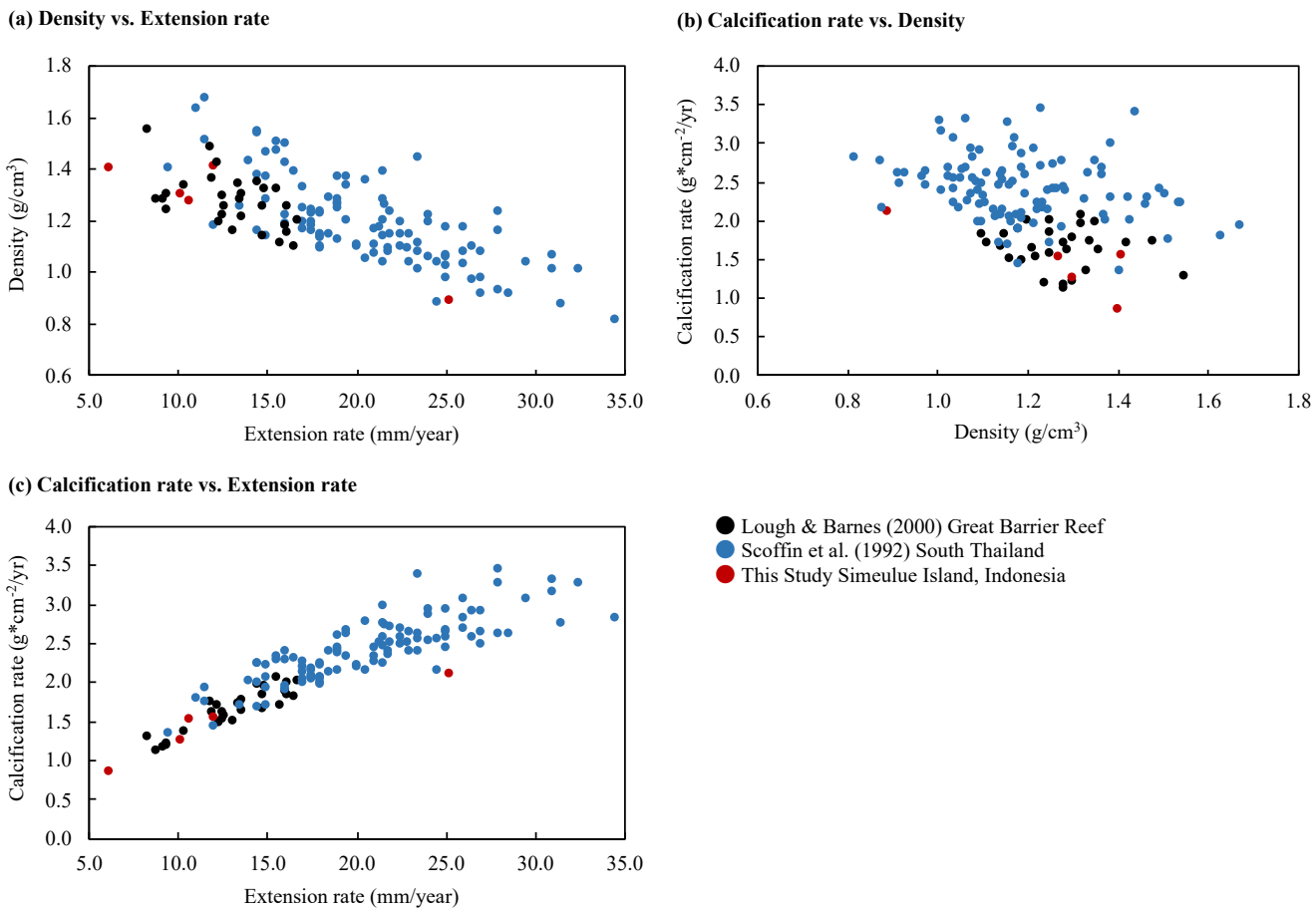

Fig. S6 Scatter diagrams of average skeletal growth data (*Porites* sp.) for the previous studies and this study.

Data is from the Great Barrier Reef (the black circles, Lough & Barnes, 2000), South Thailand (the blue circles, Scoffin et al., 1992), and Simeulue Island (the red circles, this study, mean value of each core).

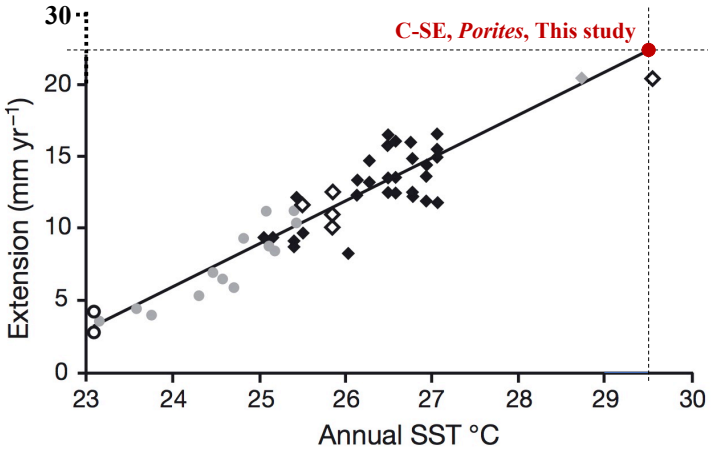

Fig. S7 Colony extension rate vs. annual SST for *Porites* corals (Goodkin et al., 2012, Fig. 6, modified). Data is from the Hawaiian archipelago (the gray circles, Grigg 1981), Phuket, Thailand (the gray diamonds, Scoffin et al., 1992), the Great Barrier Reef (the black diamonds, Lough & Barnes 2000), the Arabian Gulf and Lihir Island (the white diamonds, Lough, 2008), and Hong Kong (the white circles, Goodkin et al., 2012). The red circle shows the C-SE *Porites* core in this study (x: 29.5 ℃, y: 25.26 mm/year). The regression line excepts Goodkin et al. (2012) and this study.

226 References

227 Al-Rousan, S., Felis, T., Manasrah, R. and Al-Horani, F. (2007) Seasonal variations in the stable oxygen isotopic
228 composition in *Porites* corals from the northern Gulf of Aqaba, Red Sea. *Geochem. J.* **41**(5), 333-340.

229 Carriquiry, J. D., Risk, M. J. and Schwarcz, H. P. (1994) Stable isotope geochemistry of corals from Costa Rica
230 as proxy indicator of the El Niño/Southern Oscillation (ENSO). *Geochim. Cosmochim. Acta*. **58**(1), 335-351.

231 Cole, J. E. and Fairbanks, R. G. (1990) The Southern Oscillation recorded in the $\delta^{18}O$ of corals from Tarawa
232 Atoll. *Paleoceanography*. **5**(5), 669-683.

233 Cahyarini, S. Y., Pfeiffer, M., Timm, O., Dullo, W. C. and Schönberg, D. G. (2008) Reconstructing seawater
234 $\delta^{18}O$ from paired coral $\delta^{18}O$ and Sr/Ca ratios: Methods, error analysis and problems, with examples from
235 Tahiti (French Polynesia) and Timor (Indonesia). *Geochim. Cosmochim. Acta*. **72**(12), 2841-2853.

236 Goodkin, N. F., Switzer, A. D., McCorry, D., DeVantier, L., True, J. D., Hughen, K. A., Angeline, N. and
237 Yang, T. T. (2011) Coral communities of Hong Kong: long-lived corals in a marginal reef environment. *Mar.*
238 *Ecol. Prog. Ser.* **426**, 185-196.

239 Juillet-Leclerc, A. and Schmidt, G. (2001) A calibration of the oxygen isotope paleothermometer of coral
240 aragonite from *Porites*. *Geophys. Res. Lett*. **28**(21), 4135-4138.

241 Lough, J. M. and Barnes, D. J. (2000) Environmental controls on growth of the massive coral *Porites*. *J. Exp.*
242 *Mar. Biol. Ecol.* **245**(2), 225-243.

243 McCulloch, M. T., Tudhope, A. W., Esat, T. M., Mortimer, G. E., Chappell, J., Pillans, B., Chivas, A. R. and
244 Omura, A. (1999) Coral record of equatorial sea-surface temperatures during the penultimate deglaciation at
245 Huon Peninsula. *Science*, **283**(5399), 202-204.

246 Morimoto, M., Abe, O., Kayanne, H., Kurita, N., Matsumoto, E. and Yoshida, N. (2002) Salinity records for the
247 1997–98 El Nino from Western Pacific corals. *Geophys. Res. Lett*. **29**(11), 35-1.

248 Nagtegaal, R., Grove, C. A., Kasper, S., Zinke, J., Boer, W. and Brummer, G. J. A. (2012). Spectral

luminescence and geochemistry of coral aragonite: Effects of whole-core treatment. *Chem. Geol*. **318**, 6-15.

Scoffin, T. P., Tudhope, A. W., Brown, B. E., Chansang, H. and Cheeney, R. F. (1992) Patterns and possible environmental controls of skeletogenesis of *Porites lutea*, South Thailand. *Coral Reefs*, **11**(1), 1-11.

Watanabe, T., Winter, A. and Oba, T. (2001) Seasonal changes in sea surface temperature and salinity during the Little Ice Age in the Caribbean Sea deduced from Mg/Ca and $^{18}O/^{16}O$ ratios in corals. *Mar. Geol.* **173**, 21-35.

Watanabe, T. K., Watanabe, T., Yamazaki, A., Pfeiffer, M., Garbe-Schönberg, D. and Claereboudt, M. R. (2017) Past summer upwelling events in the Gulf of Oman derived from a coral geochemical record. *Scientific reports*, **7**(1), 4568.